Supporting Information

Probing the effect of the Pt-Ni-Pt(111) bimetallic surface electronic structures on the ammonia decomposition reaction‡

Jian-Qiang Zhong[a,b,c,*,†], Xiong Zhou[a,c], Kaidi Yuan[b,c], Christopher A. Wright[d], Anton Tadich[d,e], Dongchen Qi[d], He Xing Li[f], Kai Wu[c,g], Guo Qin Xu[a,c,h], and Wei Chen[a,b,c,h,*]

[a] Department of Chemistry, National University of Singapore, 3 Science Drive 3, 117543, Singapore
[b] Department of Physics, National University of Singapore, 2 Science Drive 3, 117542, Singapore
[c] Singapore-Peking University Research Centre (SPURc), 1 CREATE Way, #15-01, CREATE Tower, 138602, Singapore
[d] Department of Chemistry and Physics, La Trobe Institute for Molecular Science, La Trobe University, Melbourne, Victoria, 3086, Australia
[e] Australian Synchrotron, Clayton, Victoria, 3168, Australia
[f] Chinese Education Ministry Key Laboratory of Resource Chemistry, Shanghai Normal University, Shanghai, 200234, China
[g] College of Chemistry and Molecular Engineering, Peking University, Beijing, 100871, China
[h] National University of Singapore (Suzhou) Research Institute, 377 Lin Quan Street, Suzhou Industrial Park, Jiangsu, 215123, China

1. Experimental details

The main experiments were carried out in a SPECS NAP-XPS system.

The surfaces of Pt(111) and Ni(111) (MaTeck) single crystals were cleaned by cycles of Ar^+ sputtering and high temperature annealing in a home-built preparation chamber (base pressure of 2×10^{-10} mbar), which was connected to the NAP-XPS system through a gate valve. Ion sputtering (cold cathode ion sputter source, Omicron, ISE 5) was conducted under the Ar pressure of ~ 1.6×10^{-6} mbar (99.999%, CryoExpress Singapore) with 1.0 – 1.5 keV ion energies at room temperature. The single crystals were heated to 700 – 800 K in 1.0×10^{-7} mbar oxygen environment (99.999%, CryoExpress Singapore) for 2 minutes and then flashed to 1100 K. These procedures were repeated until surface cleanliness was verified with invisible C 1s and O 1s signals by the XPS measurements.

The Pt-Ni-Pt(111) bimetallic structures were prepared by depositing Ni (99.98%, Alfa Aesar) on the clean Pt(111) surface through an e-beam evaporator (EFM 3, Omicron). The nominal thickness of the Ni was estimated from a calibrated flux monitor, which was located at the exit of the evaporator column, and was further estimated from the attenuation of the Pt 4f intensity. The Ni-Pt(111) samples were then annealed at 800 K for 5 minutes to form well-ordered Pt-Ni-Pt(111) bimetallic structures. The low energy electron diffraction (LEED) patterns were also obtained at the same preparation chamber (SPECTALEED optics, Omicron).

The NAP-XPS measurements were conducted in the analysis chamber (base pressure of 2×10^{-10} mbar) which consists of an *in-situ* NAP-cell and a SPECS PHOIBOS 150 NAP. The PHOIBOS 150 NAP has a three-stage differentially pumped electrostatic pre-lens and a PHOIBOS 150 analyzer with a 1D-DLD detector. The retractable high-pressure cell (up to 25 mbar) can be docked to the front aperture of the PHOIBOS 150 NAP analyzer for NAP-XPS measurements. The reachable sample temperatures in the cell are from 200 K to 900 K through either liquid nitrogen cooling or e-beam heating. The analysis chamber was equipped with a twin anode X-ray source (SPECS XR 50, Al K_α, $h\nu$ = 1486.6; Mg K_α, $h\nu$ = 1253.6 eV).

NH_3 (99.99995%, Showa Denko) was introduced into the NAP-cell through a leak valve. The pressure was maintained at 0.6 mbar and the sample surface temperature was progressively ramped up during the measurements. Reacted gases were analyzed by a quadruple mass spectrometer (RGA100, SRS) in the NAP lens chamber.

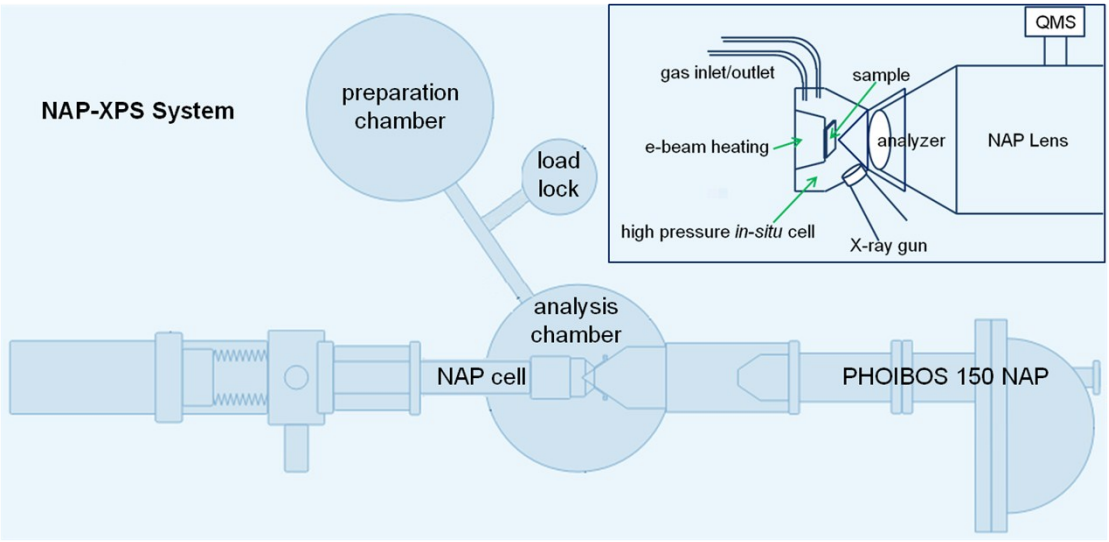

Figure S1. Schematic diagram of the NAP-XPS system. Inset shows the *in-situ* NAP-cell docked to the analyzer. The X-rays penetrate a 100 nm Si_3N_4 window to reach the

sample. The photoelectrons were detected by the PHOIBOS 150 NAP electron analyzer through a nozzle with a diameter of 300 μm. Reacted gases were analyzed by a quadruple mass spectrometer attached to the NAP lens chamber.

2. Quadruple mass spectrometer and the N_2 formation rate estimation (mol/min)

We used the quadruple mass spectrometer to analyze the reacted gases during the NAP-XPS measurements simultaneously. In our experiments, NH_3 was introduced into the NAP cell through the gas inlet while the gas outlet was closed, the nozzle (300 um) was considered as a kind of gas outlet for analyzing various reacted gases. Considering the nearly constant outlet pressure (NAP chamber, $\sim 1\times10^{-5}$ mbar) and pumping speed (HiPace 700, Pfeiffer), the N_2 formation rate can be roughly expressed as

$$r = \text{pumping speed} \times \text{outlet pressure} \times N_2 \text{ mole fraction}, \qquad \text{(L/s mbar)}$$

By applying the ideal gas equation,

$$pV = nRT,$$

the gas formation rate can be converted to mol/min. This is possible due to the closed system conditions with a small volume where a simple chemical reaction takes place.

For clear comparisons between different experiments, the derived formation rate (r) was further normalized by dividing the NH_3 mole fraction

$$r_{norm} = r/NH_3 \text{ mole fraction}, \qquad \text{(mol/min)}$$

In the main paper, we presented the N_2 formation rate extracted as described above.

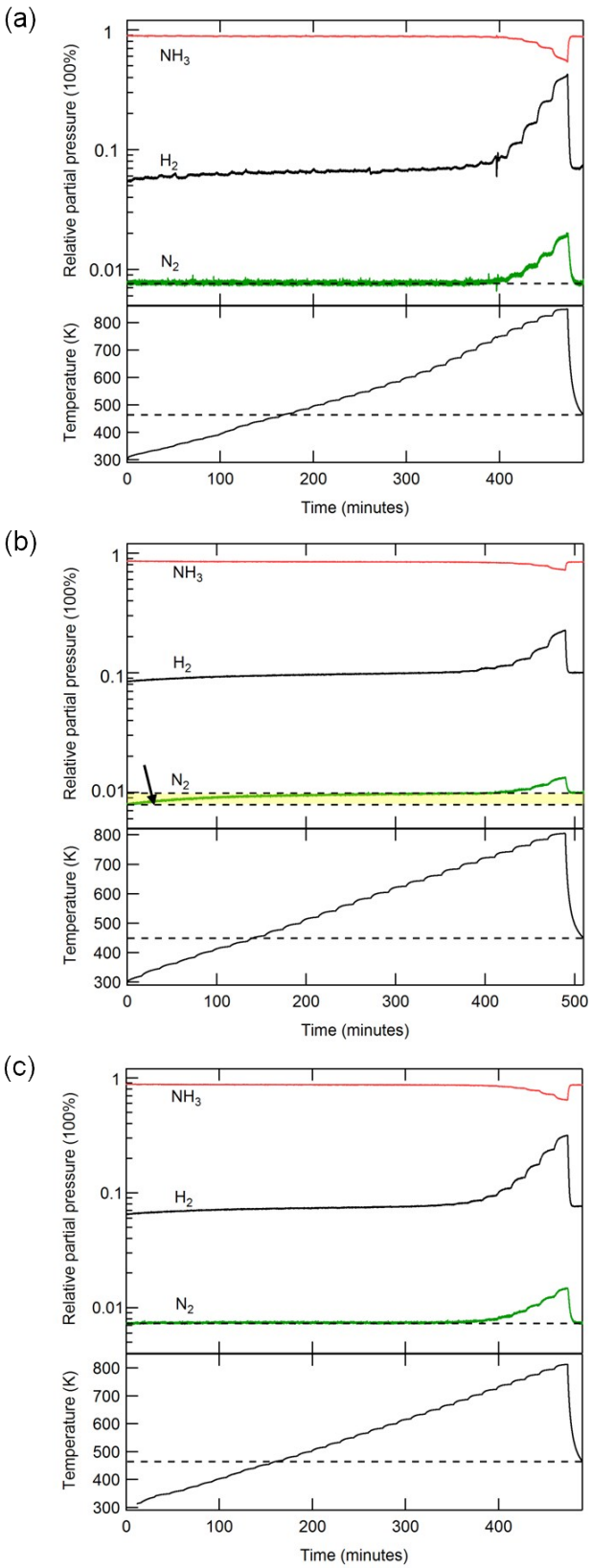

Figure S2. QMS reactivity data during the NH_3 decomposition for (a) Pt(111), (b) Pt-Ni-Pt(111) and (c) Ni(111).

3. Surface structures: Pt(111), Pt-Ni-Pt(111) and Ni(111)

The surface structures of Pt(111), Pt-Ni-Pt(111) and Ni(111) were also investigated by LEED measurements. The growth mode of Ni on Pt(111) at room temperature has been identified to be an island growth model with initial nucleation at the step edges of the Pt(111) surface.[1] Kitchin *et al.* also pointed out that the annealing process at 640 K results in a smoother surface accompanied with Ni diffusing into the bulk of the crystal as observed from the scanning tunneling microscopy (STM) and auger electron spectroscopy (AES) measurements. Gauthier *et al.* firstly reported an compositional oscillation of the Pt_xNi_{1-x}(111) alloy across the three outermost layers.[2] Upon annealing, the topmost alloy layer contains almost pure Pt atoms and the subsurface layers are Ni-rich (Figure S3).

For the studies presented here, several types of Pt-Ni-Pt(111) bimetallic samples were prepared. Upon depositing 1.1, 1.3, 1.4, 2.7 and 2.9 ML Ni onto the clean Pt(111), the surfaces were subsequently annealed at 800 K for 5 minutes, resulting in two surface structures with the LEED patterns shown in Figure S4 and Figure S5. For low coverage (i.e., less than 2 ML) Ni on Pt(111), the LEED pattern remains 1×1 reflections, corresponding to the same reciprocal lattice vectors as the Pt(111) substrate, while these LEED spots split into two after the annealing process. The LEED patterns of higher coverage (i.e., more than 2 ML) Ni on Pt(111) are more complex, featuring satellite spots around 1×1 diffraction spots from the Pt(111) substrate. After annealing at 800 K, the LEED spots further split into three at the original 1×1 spot locations as shown in Figure S5(c).

The surface symmetry obtained from LEED and STM analyses show that the segregated Ni sub-layer will undergo different reconstructions depending on the amount of Ni atoms (Figures S3 – S5). This is understandable since the Pt-Pt bond length (2.79 Å) is about 12% larger than that of Ni-Ni (2.49 Å).[1] The lattice mismatch between the Pt top-layer and Ni sub-layers can certainly cause the so-called commensurate-incommensurate phase transitions.[3] The splitting of the LEED spots in Figures S4(c) and S5(c) can be correlated with the different orientations of the subsurface Ni as discussed in the paper.[4]

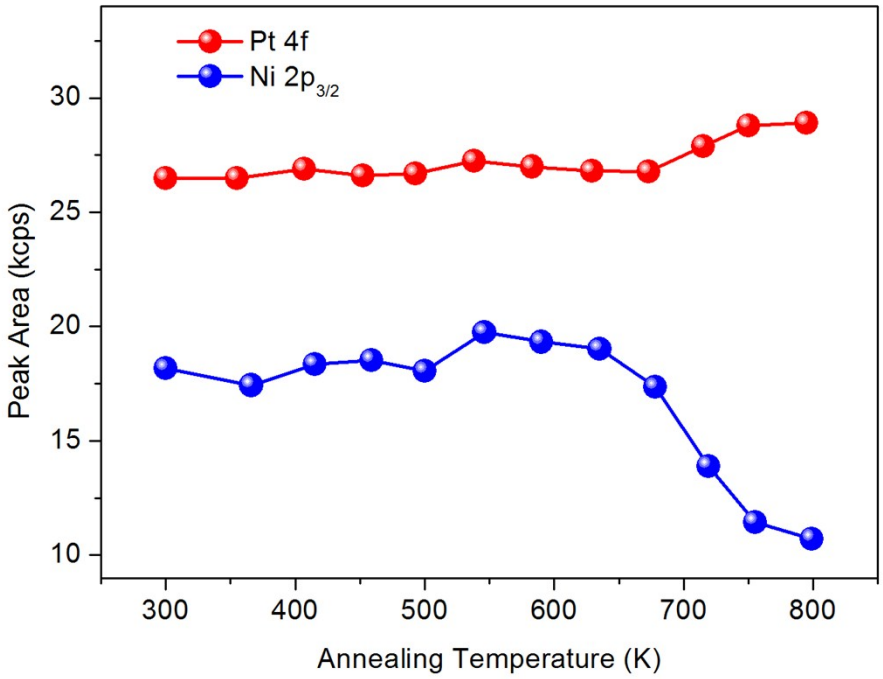

Figure S3. The effects of annealing temperatures on 2.9 ML Ni film on Pt(111).

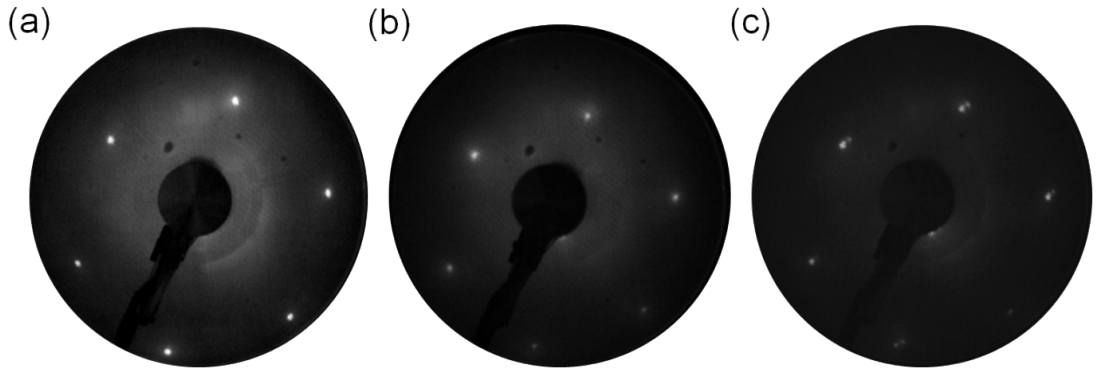

Figure S4. LEED patterns for (a) a clean Pt(111) surface, (b) after depositing 1.1 ML Ni on Pt(111), and (c) annealing (b) at 800 K (E = 83 eV).

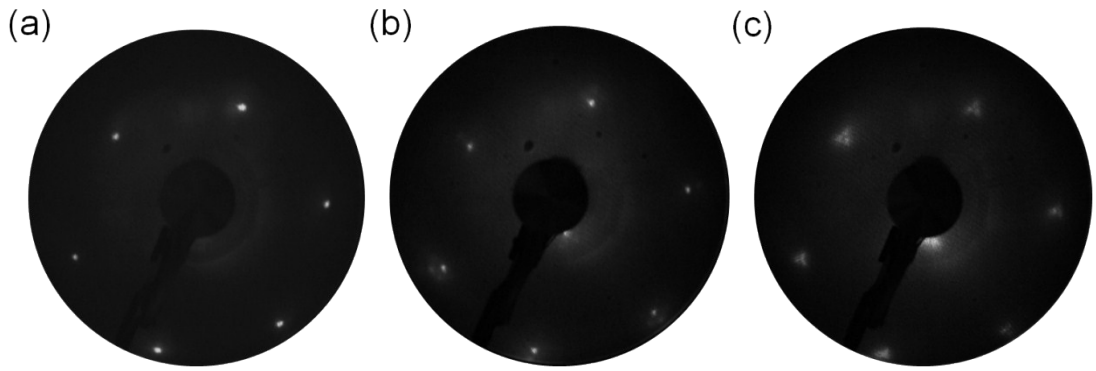

Figure S5. LEED patterns for (a) a clean Pt(111) surface, (b) after depositing 2.9 ML Ni on Pt(111), and (c) annealing (b) at 800 K (E = 80 eV).

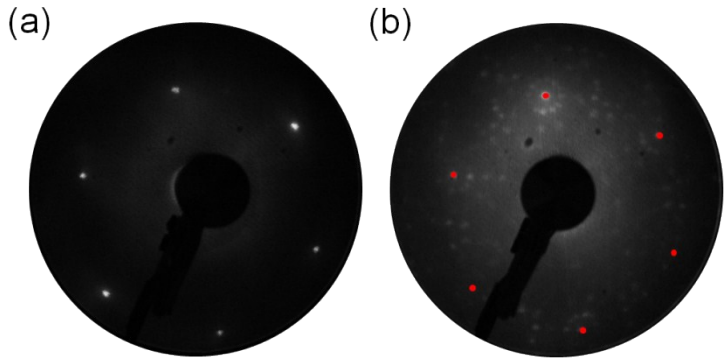

Figure S6. LEED patterns for (a) a clean Ni(111) surface, (b) after the NH_3 decomposition reaction (a nickel nitride layer was formed) (E = 72 eV).

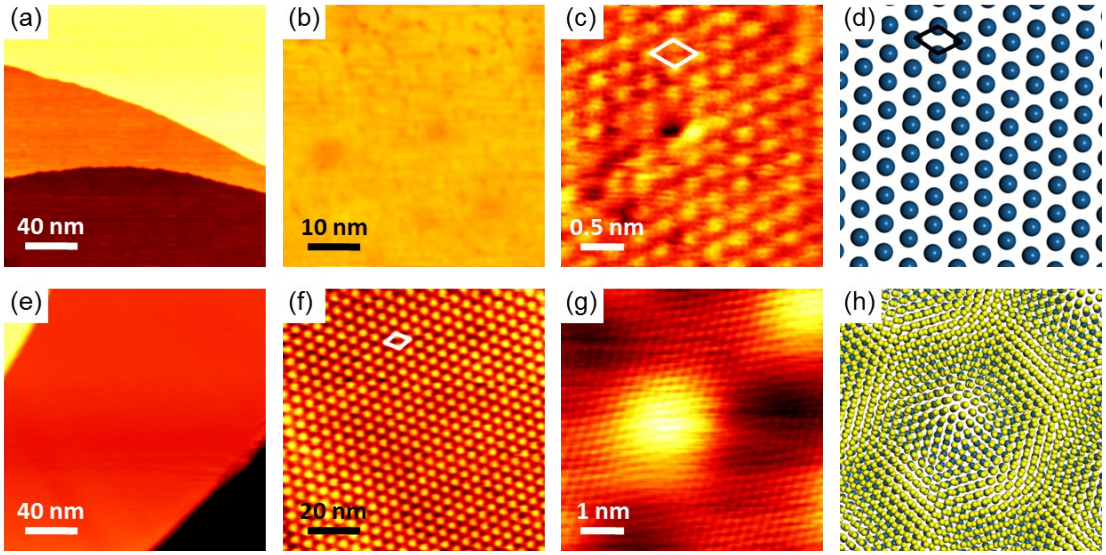

Figure S7. STM images of clean Pt(111) and Ni layers covered Pt(111). (a, b) Large scale STM images of clean Pt(111) (V = 1 V, I = 100 pA). (c) Atomic resolved STM image of Pt(111). Unit cell: 0.28 ± 0.01 nm (V = -50 mV, I = 30 nA). (d) Corresponding atomic models for (c). (e, f) Large scale STM images of Ni-Pt(111) (V = 0.1 V, I = 100 pA). Unit cell of Moire pattern: 4.7 ± 0.1 nm. (g) Atomic resolved STM image of Ni-Pt(111). Unit cell: 0.23 ± 0.02 nm (V = -40 mV, I = 80 nA). (h) Corresponding atomic models for (g).

4. Additional NAP-XPS spectra

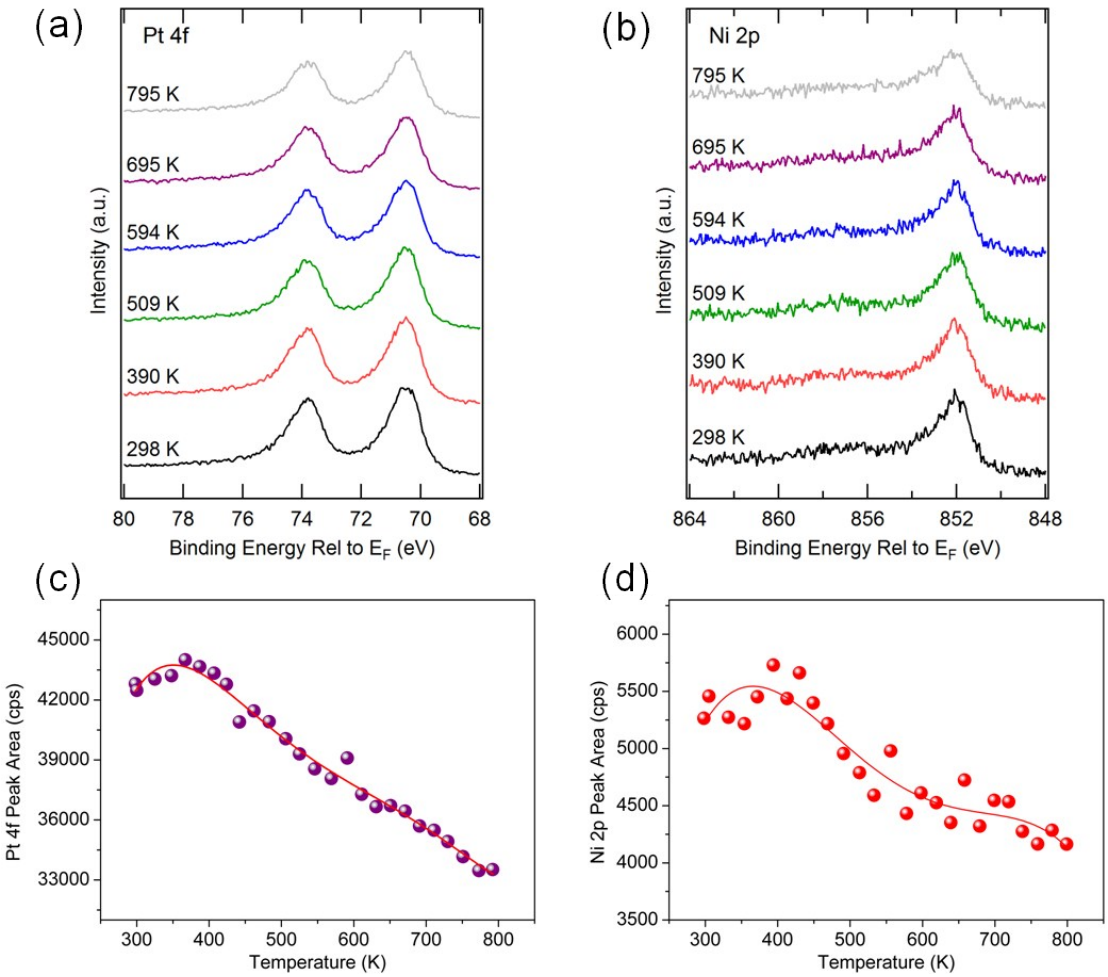

Figure S8. (a) Pt 4f and (b) Ni 2p core level spectra ($h\nu$ = 1253.6 eV) acquired during NH_3 decomposition under 0.6 mbar of NH_3 on Pt-Ni-Pt(111) with 1.3 ML Ni. (c) and (d) are the corresponding evolutions of the peak intensities during the catalytic decomposition of NH_3.

The intensities of Pt 4f and Ni 2p are decreased by ~ 23% and ~ 22% respectively due to the increased coverage of the reaction intermediates. The similar attenuations of the Pt 4f and Ni 2p demonstrate the stability of the sandwich structure. The slightly increased intensities around 400 K could be attributed to NH_x recombinative desorption induced by the weakened Pt-N bonding at the second reaction stage as depicted in Figure 2.

5. Explanations for the spectral shape variations in Figure 5(a)

Detailed inspections of the Ni 2p in Pt-Ni-Pt(111) bimetallic surface (Figure 5(a)) also revealed a new fine structure appearing at the higher binding energy of the main peak. The possible reason of two chemically inequivalent atoms (i.e., surface and

subsurface Ni atoms) can be excluded since almost all Ni atoms have already been diffused into the subsurface layer after annealing at 800 K.

Here, the well-developed "two hole state" theory was adopted to account for the evolution of these peaks: the appearance of a new fine structure peak and a large negative shift of the satellite peak.[5] The initial state of a clean Ni metal is $c3d^94s$ (c denotes a core level), where the $3d^9$ states lie within the wide 4s band across the Fermi level. Upon photon-ionization, an instantaneously produced Columbic potential pulls the conduction band ($3d^94s$) below the Fermi level. Delocalized electrons from the Fermi level will then fill either $3d^9$ hole states or 4s hole states during the lifetime of the core hole. As a result, two final states occur: $c^{-1}3d^{10}4s$ (main peak, c^{-1} denotes a core hole) and $c^{-1}3d^94s^2$ (satellite peak). The binding energy difference between these two states comes from different screening effects (filled 3d states release greater relaxation energy than the filled 4s states, the $c^{-1}3d^94s^2$ state is an excited state with an excitation energy of ~ 6 eV).[5] However, upon annealing, Ni atoms diffused into the subsurface layers, resulting in changes in coordinative bonding with surrounding Pt atoms. The variations in the spectral shape (i.e., the emerging of a fine structure peak) can be understood through two $c^{-1}3d^{10}4s$ final state configurations via local screening and non-local screening.[6, 7] The main peak was attributed to the screening from nearest Pt neighbors and the process was written as $c3d^94s \rightarrow c^{-1}3d^{10}4sL$, where L denotes a hole in Pt valence band after charge transfer (i.e., local screening). The new fine structure peak was then corresponds to a $c3d^94s \rightarrow c^{-1}3d^{10}4sL^*$ process, where the screening is provided by neighboring $NiPt_x$ units (none-local screening). Due to the increased attractive interactions between Ni and Pt atoms in the Pt-Ni-Pt(111) surface alloys, the excitation energy upon photon-ionization for the $c^{-1}3d^94s^2$ state was also largely decreased, resulting a negative shift of the satellite peak. The relative intensity of the fine structure according to the scheme discussed above can be composition dependent for annealed bimetallic surfaces. For Pt-Ni-Pt(111) with 2.7 ML Ni, the fine structure peak is much more pronounced due to the abundance of $NiPt_x$ units (Figure S9(a) and Figure S10(a)). This analysis is in good agreement with previous studies of NiO surfaces and Pd-Mn bimetallic surfaces.[6, 7]

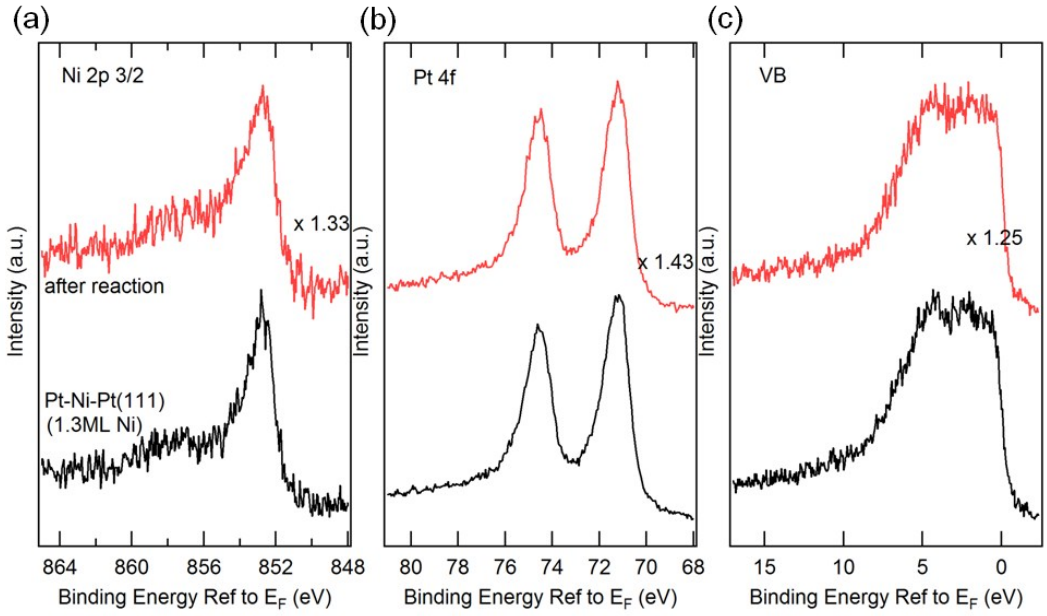

Figure S9. XPS spectra acquired before and after NH_3 decomposition on Pt-Ni-Pt(111) with 1.3 ML Ni. (a) Ni 2p, (b) Pt 4f, and (c) XPS valence band.

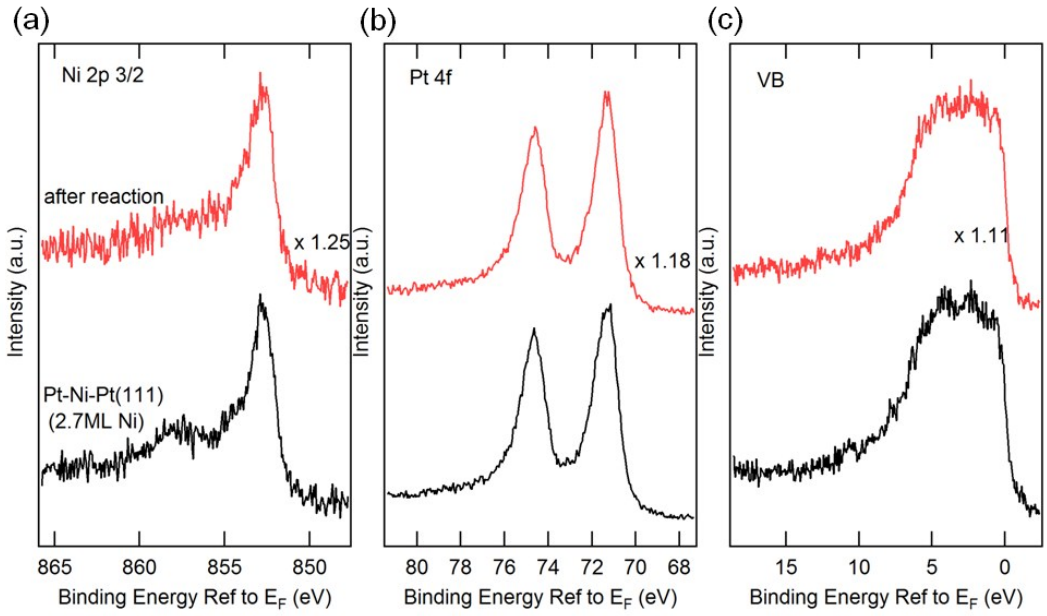

Figure S10. XPS spectra acquired before and after NH_3 decomposition on Pt-Ni-Pt(111) with 2.7 ML Ni. (a) Ni 2p, (b) Pt 4f, and (c) XPS valence band.

References:

1. Kitchin, J. R.; Khan, N. A.; Barteau, M. A.; Chen, J. G.; Yakshinskiy, B.; Madey, T. E., Elucidation of the active surface and origin of the weak metal–hydrogen bond

on Ni/Pt(111) bimetallic surfaces: a surface science and density functional theory study. *Surf. Sci.*2003, 544, 295-308.
2. Gauthier, Y.; Baudoing, R.; Joly, Y.; Rundgren, J.; Bertolini, J. C.; Massardier, J., PtxNi1−x(111) alloy surfaces: structure and composition in relation to some catalytic properties. *Surf. Sci.* 1985, 162, 342-347.
3. Andryushechkin, B. V.; Cherkez, V. V.; Kierren, B.; Fagot-Revurat, Y.; Malterre, D.; Eltsov, K. N., Commensurate-incommensurate phase transition in chlorine monolayer chemisorbed on Ag(111): Direct observation of crowdion condensation into a domain-wall fluid. *Phys. Rev. B* 2011, 84, 205422.
4. Farid El, G.; Juan, M. P.; Christof, K.; Angela, S.; Andreas, K. S.; Kevin, F. M.; Jorge, I. C.; Juan de la, F., Structure and morphology of ultrathinCo/Ru(0001) films. *New J. Phys.* 2007, 9, 80.
5. Hüfner, S., *Photoelectron Spectroscopy: Principles and Applications*. Springer Berlin Heidelberg: 1995; Vol. 82.
6. Sandell, A.; Jaworowski, A. J., The Mn 2p core-level photoelectron spectrum of Pd–Mn bimetallic systems on Pd(100). *J. Electron. Spectrosc. Relat. Phenom.* 2004, 135, 7-14.
7. Alders, D.; Voogt, F. C.; Hibma, T.; Sawatzky, G. A., Nonlocal screening effects in 2p x-ray photoemission spectroscopy of NiO (100). *Phys. Rev. B* 1996, 54, 7716-7719.